Available online at www.sciencedirect.com

SCIENCE DIRECT®

Geomorphology 71 (2005) 402–423

GEOMORPHOLOGY

www.elsevier.com/locate/geomorph

Regional relief characteristics and denudation pattern of the western Southern Alps, New Zealand

Oliver Korup[a,*], Jochen Schmidt[b], Mauri J. McSaveney[c]

[a]*WSL Swiss Federal Institute for Snow and Avalanche Research SLF, CH-7260 Davos, Switzerland*
[b]*National Institute for Water and Atmospheric Research, Christchurch, New Zealand*
[c]*Institute for Geological and Nuclear Sciences, Lower Hutt, New Zealand*

Received 7 June 2004; received in revised form 1 April 2005; accepted 27 April 2005
Available online 5 July 2005

Abstract

The Southern Alps of New Zealand are the topographic expression of active oblique continental convergence of the Australian and Pacific plates. Despite inferred high rates of tectonic and climatic forcing, the pattern of differential uplift and erosion remains uncertain. We use a 25-m DEM to conduct a regional-scale relief analysis of a 250-km long strip of the western Southern Alps (WSA). We present a preliminary map of regional erosion and denudation by overlaying mean basin relief, a modelled stream-power erosion index, river incision rates, historic landslide denudation rates, and landslide density. The interplay between strong tectonic and climatic forcing has led to relief production that locally attains ~2 km in major catchments, with mean values of 0.65–0.68 km. Interpolation between elevations of major catchment divides indicates potential removal of 10^1–10^3 km^3, or a mean basin relief of 0.51–0.85 km in the larger catchments. Local relief and inferred river incision rates into bedrock are highest about 50–67% of the distance between the Alpine fault and the main divide. The mean regional relief variability is ±0.5 km.

Local relief, valley cross-sectional area, and catchment width correlate moderately with catchment area, and also reach maximum values between the range front and the divide. Hypsometric integrals show scale dependence, and together with hypsometric curves, are insufficient to clearly differentiate between glacial and fluvial dominated basins. Mean slope angle in the WSA ($\psi = 30^\circ$) is lower where major longitudinal valleys and extensive ice cover occur, and may be an insensitive measure of regional relief. Modal slope angle is strikingly uniform throughout the WSA ($\varphi = 38$–40°), and may record adjustment to runoff and landsliding. Both ψ and φ show non-linear relationships with elevation, which we attribute to dominant geomorphic process domains, such as fluvial processes in low-altitude valley trains, surface runoff and frequent landsliding on montane hillslopes, "relief dampening" by glaciers, and rock fall/avalanching on steep main-divide slopes.

Keywords: Southern Alps; New Zealand; Denudation; Terrain analysis; Digital elevation models; Neotectonics

* Corresponding author.
E-mail address: korup@slf.ch (O. Korup).

0169-555X/$ - see front matter © 2005 Elsevier B.V. All rights reserved.
doi:10.1016/j.geomorph.2005.04.013

1. Introduction

The increasing availability of digital elevation models (DEMs) has prompted rapid advances for regional-scale characterization and numerical modelling of mountain landscapes (e.g., Pike, 1995; Meigs and Sauber, 2000; Kühni and Pfiffner, 2001; Rasemann et al., 2002; Bishop et al., 2002, 2003; Riquelme et al., 2003; Jamieson et al., 2004). Among many other methods, geomorphometric parameters (e.g., Rasemann et al., 2002; Schmidt and Dikau, 1999; Hovius, 2000), and landform classifications (e.g., Wallace, 1995; Dikau et al., 1995; Brabyn, 1997) have been used to characterize, subdivide, and compare mountain ranges.

Morphometric variables of small alpine basins assist the prediction of dominating fluvial or debris-flow process (e.g., De Scally and Owens, 2004). Hypsometry was applied as a measure of relief production to address the question of whether rivers or glaciers would have greater erosional efficiency. In the Olympic Mountains, USA, Montgomery (2002) used valley width, relief, and cross-sectional areas, normalized by contributing catchment area, to quantify differences between fluvial and glacial relief production. Others (Kirkbride and Matthews, 1997; Brocklehurst and Whipple, 2002, 2004) used hypsometric curves and integrals (Strahler, 1952), and geophysical relief (Montgomery and Greenberg, 2000) to explore this difference. Hypsometric integrals quantify catchment topography within a single figure, and together with the shape of hypsometric curves they were used to infer lithologic, climatic, tectonic, or scale-dependent influences on basin geomorphometry (Hurtrez et al., 1999; Bishop et al., 2002). Basin shape, e.g., contained in relief and elongation ratios, among other attributes were used as indicators of tectonic forcing in Himalayan catchment evolution (Jamieson et al., 2004).

Regional slope distributions were used to infer limits to mountain relief, such as threshold hillslopes, as a function of mountain-scale rock-mass strength and fluvial incision rates (Schmidt and Montgomery, 1995; Burbank et al., 1996; Montgomery, 2001). In the NW Himalaya, the regional pattern of slope distributions, mean elevation, and hypsometry was found to be less dependent on denudation rates than on the extent of glaciation (Brozovic et al., 1997). Linking climate data with DEM analyses provides interesting results for pinpointing similar climatic forcing on mountain relief, and vice versa. For example, correlation of DEM-derived slope data with precipitation measurements led Gabet et al. (2004) to infer a climatic control on hillslope angle and relief in the Himalaya.

Analysis of river longitudinal profiles has gained especial interest, since such profiles are widely assumed to record adjustment to tectonic forcing in many uplifting mountain belts (e.g., Seeber and Gomitz, 1983; Sklar and Dietrich, 1998; Baillie and Norbu, 2004; Whipple, 2004). Equilibrium river longitudinal profiles generally are upwardly concave (Strahler, 1952). Departures from idealized curves would reflect among others, differences in rock uplift, bedrock lithology, non-fluvial erosion processes, sediment availability, impoundments, orographic precipitation effects, or other transient disturbances (Kirby et al., 2003; Snyder et al., 2003; Duvall et al., 2004; Kobor and Roering, 2004; Tucker, 2004; Whipple, 2004).

There is now a whole "family" of stream-power laws (Whipple, 2004) that are used for modelling fluvial incision into bedrock in response to external forcing. In its basic form, the stream-power model is based on hydraulic relations stating that bedrock channel incision E is a power-law function of unit stream power or basal shear stress,

$$E = KA^m S^n \tag{1}$$

where K is the erosion coefficient, A is drainage area, S is local channel slope, and m and n are empirically derive constants varying in different landscapes (Howard and Kerby, 1983). Whipple and Tucker (1999) demonstrated that $m=1/2$, $n=1$ for a stream power per unit length model, $m=1/2$, $n=1$ for a specific stream-power model, and $m=1/2$, $n=2/3$ for a shear stress model. Values of K range over several orders of magnitude, depending on lithology, climate, orograpic precipitation, and differential rock uplift (Kobor and Roering, 2004). This model subsumes a large range of variables owing to the complexity of form and process in many mountain rivers in an oversimplified and not-yet-fully tested manner (Finlayson and Montgomery, 2003). Nevertheless its simplicity makes it a convenient tool for indicating

regional variations of fluvial incision within a given mountain belt (Finlayson et al., 2002). By defining an erosion index

$$\varepsilon = EK^{-1} = A^m S^n \quad (2)$$

Finlayson et al. (2002) employed slope-area erosional indices on total stream power, unit stream power, and shear stress to indicate the spatial coincidence of high inferred erosion with young metamorphic massifs in the Himalayas.

Slope–area relationships were also proposed as the basis for a long-term colluvial erosion law, governing debris-flow prone slopes in the Middle Hills of Nepal (Lague and Davy, 2003).

Finally, global-scale analyses of DEM data highlight the non-linear relationship between mean local relief and average erosion rates for tectonically active mountain belts (Montgomery and Brandon, 2002). Finlayson and Montgomery (2003) summarized numerous caveats when using DEMs for regional-scale analyses, mainly pertaining to cartographic projection and grid resolution.

In this contribution, we focus on the western Southern Alps (WSA) of New Zealand as a prime example of a tectonically active mountain belt subject to extreme tectonic and climatic forcing (Whitehouse, 1988). Despite high documented rates of rock uplift, precipitation, and denudation, few studies so far have investigated the relief of the WSA from a regional perspective (Hovius, 2000). There are as yet not enough data warranting a differential uplift map, and the regional geology is currently being compiled at 1:250,000 scale.

Therefore our key objective is to derive from a DEM of the regional topography any characteristics or patterns that may be used for interpreting the geomorphic history of the WSA in the context of rapid uplift and erosion. Research questions that motivate our study are: What are the regional patterns of denudation in the WSA? Is there any regional pattern of slope gradients and relief which can be related to the geomorphic history? Where is bedrock incision highest at present? We attempt to answer these questions by quantitative terrain analysis and overlaying key results to provide a first regional map of erosion and denudation in the WSA.

2. The western Southern Alps, New Zealand

The western Southern Alps (WSA) form the backbone of South Island, New Zealand (Fig. 1). They lie on the boundary between the Pacific and Australian plates, which obliquely converge along the 800-km long Alpine fault (Norris and Cooper, 2000). Dextral transpression has led to exhumation of metamorphic hangingwall schists from depths of >20 km and topographic rise of the Southern Alps since 5 My (Sutherland, 1995). The metamorphic grade decreases away from garnet–oligoclase facies near the Alpine fault to quartzofeldspathic argillite–greywacke towards the main divide (Craw et al., 2003). Permian ultramafites of the Dun Mountain Group mark an accreted terrane boundary in the Cascade River catchment.

Koons (1989, 1990) made significant contributions to the understanding of the evolution of the Southern Alps by numerically modelling the interaction between tectonic uplift and denudation. His concept of an asymmetric erogenic wedge with rapid uplift and erosion on the western windward side proved consistent with the thermal history (Batt and Braun, 1999). Tippett and Kamp (1995) noted a high correlation between elevation parameters and uplift rates derived from apatite fission track analysis west of the main divide. Uplift rates are highest near the Alpine Fault Zone near Franz Josef Glacier (~10 mm y^{-1}), and appear to be matched by denudation of the same order of magnitude (e.g. Basher et al., 1988). Dip-slip rates along the Alpine fault decrease SW-ward to virtually nil at the southern end of the study area (Norris and Cooper, 2000). However, there remains uncertainty on the spatial pattern of differential uplift.

The mountain belt forms a barrier to moisture-bearing winds from the Tasman Sea, causing extreme precipitation of up to 15 m y^{-1} west to the main divide (Henderson and Thompson, 1999).

The Southern Alps and their western piedmont were extensively glaciated during the Pleistocene, and some of the terminal moraines are now situated below sea level. The precipitation divide was mobile before and during the Quaternary, when large valley glaciers flowed eastwards from centres of high precipitation in the WSA (Craw et al., 2003). Glacial transfluence occurred for instance at low-lying Haast

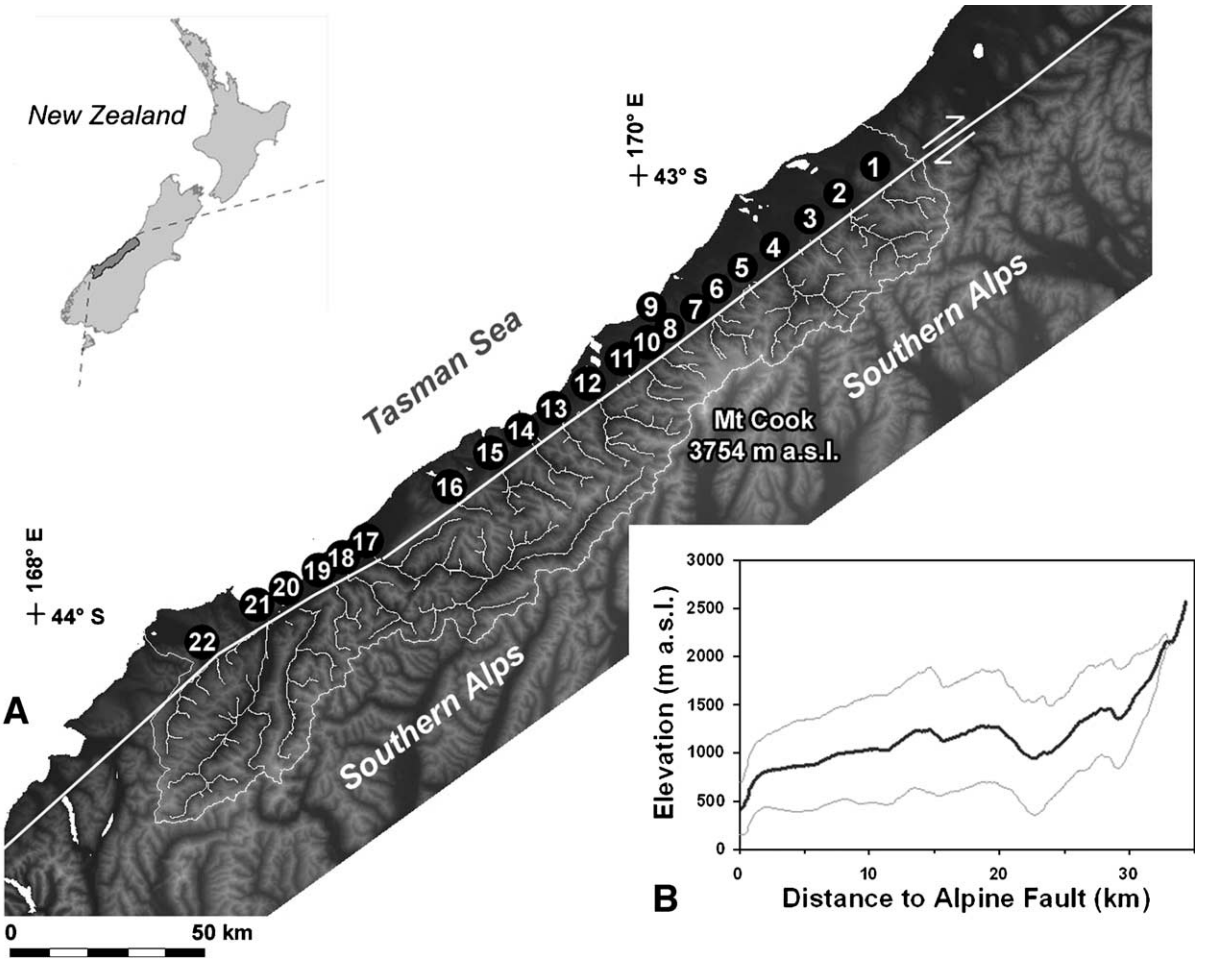

Fig. 1. A. Study area of the western Southern Alps (WSA) bounded by the Alpine fault (white line). Numbers refer to major catchments (Table 1). B. Topographic swath profile between the Alpine fault and the main divide for the study area. Thick black and thin grey lines indicate mean, and ± 1 standard deviation (S.D.) from the mean, respectively.

Pass (563 m a.s.1.) on the main divide, in the Haast-Landsborough basin. Glaciers presently cover 11% of the WSA, although their extent varies considerably from nil (Moeraki, Okuru) to 47% (Fox). Major ice fields are located in the upper Waiho and Fox basins (Fig. 2) and the Mt Aspiring massif at the head of Waiatoto River.

The WSA are drained by steep, and densely spaced, high-energy mixed bedrock/gravel-bed rivers, with low flood-discharge variability for a large range of recurrence intervals (McKerchar and Pearson, 1989). Episodic M ~8 earthquakes along the Alpine fault (200–300 y; Wells et al., 1999) rejuvenate these rivers, while uplift is continuous from near the main divide. Deeply incised v-shaped valleys are flanked by steep, rectilinear slopes, serrated ridges, and rugged tops (Whitehouse, 1988). Many of the major trunk valley have been backfilled upstream of their alluvial fans. Valley fills, mainly consisting of debris fans, alluvial flats, and terraces, cover up to ~25% (11% on average) of the areas of major alpine catchments (Fig. 2).

Postglacial landscape modification is less pronounced in the adjoining Fiordland Mountains, where rock-mass strength is higher (Augustinus, 1992). Surface runoff and landsliding are the dominant erosional

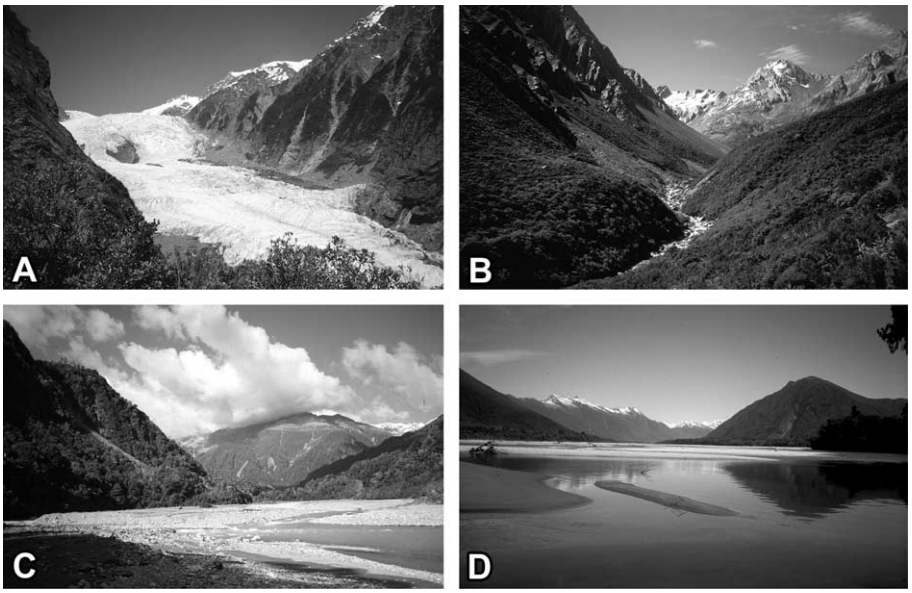

Fig. 2. Upstream views of typical valley morphologies in the WSA. A. Franz Josef Glacier from Roberts Point, Waiho valley. B. Fluvial incision into rock fall/snow avalanche cones, upper Copland valley, with main divide of the Southern Alps in background. C. Alluvial reach on lower Wanganui River. D. Broad valley train of lower Arawhata River downstream of the Alpine fault.

agents in the WSA (Hovius et al., 1997; Korup, 2005a), causing clearly visible scars in the dense montane forest cover. Denudation by these shallow landslides was estimated at 9.1 ± 5.1 mm y^{-1} for 13 basins between the Waitaha and Moeraki Rivers, fashioning sediment discharges of $1.2 \pm 0.5 \times 10^6$ m^3 y^{-1} (Hovius et al., 1997; Table 1).

3. Methodology

For this study we used a 25-m grid DEM derived from 20-m contours. The original contour base has a nominal error of ± 10 m horizontally and vertically, and is of sufficient quality for a regional-scale analysis of mountain relief. We focus here on a 250-km strip of the WSA between Waitaha and Casacade Rivers (42°57′–44°30′ S, 168°16′–170°56′ E; Fig. 1). Data on 22 mainly transverse catchments with areas A between 11 and 1313 km^2 (total 5679 km^2) were extracted from the DEM by defining their basin outlets at the Alpine fault (Table 1), using a standard single flow-direction algorithm performed on the filled grid. Hypsometric curves and integrals were calculated following the method outlined in Brocklehurst and Whipple (2004; see also for a detailed review).

We extracted river longitudinal profiles following the method of Kirby et al. (2003) by computing downstream flow length, and intersecting it with 10-m contours that were interpolated from the DEM. From the river profiles we manually extracted major convex and concave knickpoints and recorded their downstream flow distance from the Alpine fault. Using shaded-relief images and slope-map overlays, we also sampled the elevation of 61 strath and fill terrace treads above present channel beds at an estimated vertical precision of ± 3 m.

Five transverse topographic swath profiles between the Alpine fault and the main divide were computed from the DEM (Fig. 3). Our idea behind this sampling strategy is that any tectonic signal emanating from the Alpine fault may be recorded in such swaths. The same may also apply for precipitation-driven changes potentially subject to a NW–SE gradient (Henderson and Thompson, 1999). Each sampling corridor had a width of 20 km and was also used for examining trends in slope and local relief with increasing distance from the Alpine fault. An additional swath was run along

Table 1
Morphometric characteristics for major catchments in the western Southern Alps (WSA)

Catchment	Area, A (km^2)	Min. elevation, E_{min} (m a.s.l.)	Max. elevation, E_{max} (m a.s.l.)	Relief, H (m)	Mean elevation (m a.s.l.)	Hypsometric integral	Denudation rate, D (mm y^{-1})[a]	Sediment discharge, Q_s (Mm^3 y^{-1})[a]	Native forest (%)	Bare ground[b] (%)	Bare ground (%)	Glaciers (%)
Waitaha	134.0	118	2600	2482	1209	0.440	11.6	1.7	25	35	29	6
Wanganui	342.7	89	2640	2551	1202	0.436	6.1	2.1	36	40	27	13
Poerua	63.9	119	2441	2322	1147	0.443	18.1	1.2	47	23	20	3
Whataroa	452.9	80	3020	2940	1202	0.382	11.4	1.1	33	43	30	13
Waitangitaona	73.3	83	2144	2061	828	0.362	18.1	1.1	48	12	10	1
Tatare	27.7	158	2186	2028	1103	0.466	–	–	32	25	18	7
Waiho	163.8	155	3100	2945	1510	0.460	12.2	2	15	67	28	40
Omoeroa	10.6	313	1986	1673	1115	0.480	–	–	43	10	7	3
Waikukupa	24.1	213	2340	2127	1252	0.488	–	–	39	28	15	12
Fox	91.6	179	3488	3309	1629	0.438	7.5	0.71	12	72	15	47
Cook	130.7	108	3480	3372	1295	0.352	5.8	0.79	27	42	25	17
Karangarua	361.0	36	3140	3104	1154	0.360	3.7	1.3	30	35	24	11
Makawhio	114.0	32	2380	2348	1024	0.423	9.9	1.1	35	21	19	2
Mahitahi	153.1	29	2643	2614	958	0.355	6.3	0.98	36	21	19	5
Paringa	225.8	23	2626	2603	861	0.322	5.5	1.3	49	13	9	4
Moeraki	62.4	57	1900	1843	785	0.395	1.8	0.12	63	1	1	0
Haast	1313.2	12	2740	2728	978	0.354	–	–	47	19	14	4
Okuru	214.8	19	2000	1981	830	0.410	–	–	47	6	5	0
Turnbull	147.3	37	2060	2023	975	0.464	–	–	34	17	16	1
Waiatoto	441.7	11	3033	3022	1015	0.332	–	–	35	28	17	11
Arawhata	757.3	10	3019	3009	878	0.289	–	–	49	28	16	12
Cascade	242.5	33	1951	1918	847	0.424	–	–	38	21	20	1
Mean	**252.2**	**87**	**2587**	**2500**	**1082**	**0.403**	**9.1**	**1.19**	**37**	**28**	**18**	**10**
S.D.	**296.5**	**78**	**494**	**504**	**220**	**0.056**	**5.1**	**0.53**	**12**	**18**	**8**	**12**
S.E.	**63.2**	**17**	**105**	**108**	**47**	**0.012**	**1.4**	**0.15**	**2**	**4**	**2**	**3**
Median	**150.2**	**69**	**2613**	**2517**	**1064**	**0.416**	**7.5**	**1.1**	**36**	**24**	**17**	**5**

See Fig. 1 for number-coded locations. [a]Estimated from historic aseismic landslides (Hovius et al., 1997). [b]Including glaciers.

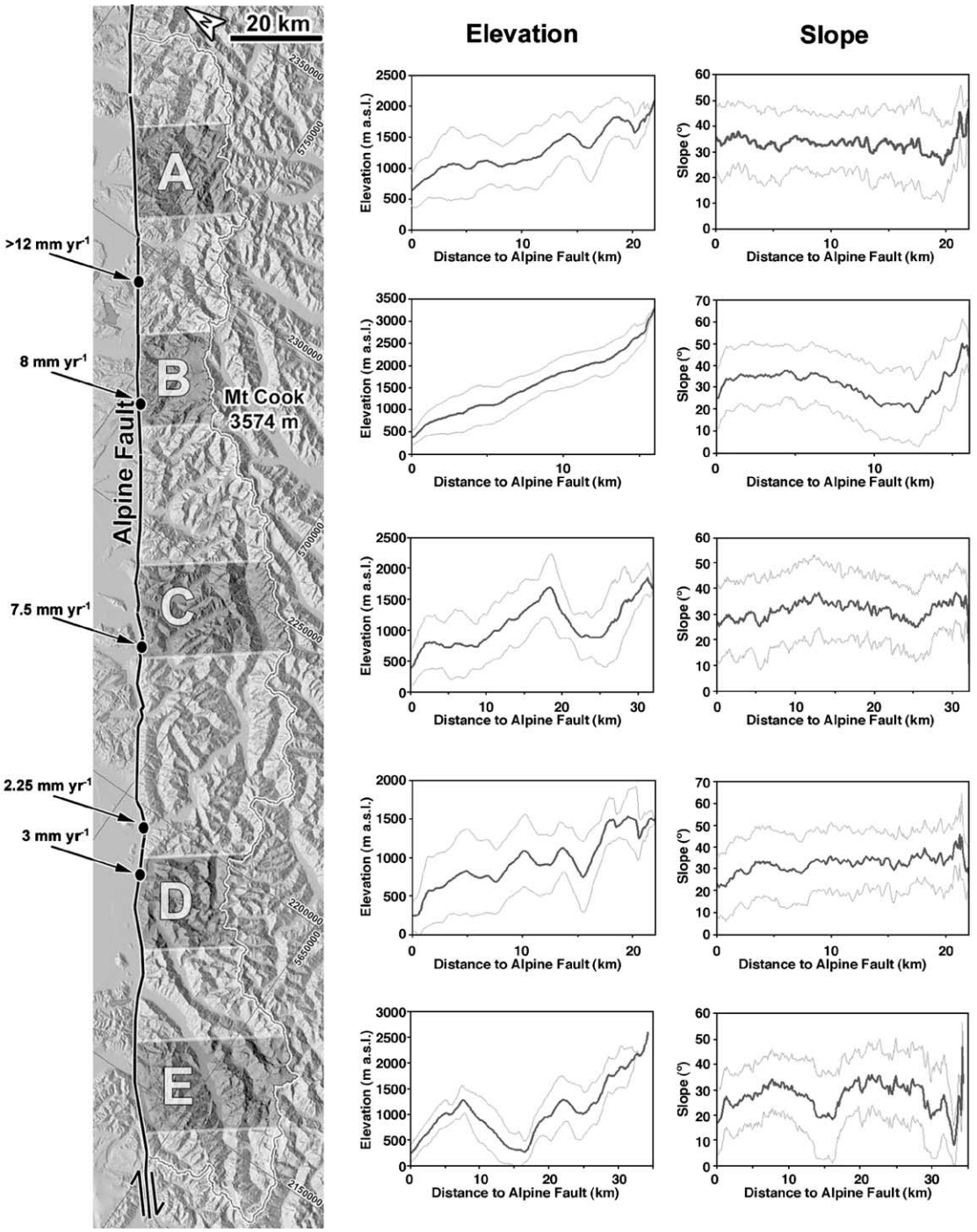

Fig. 3. Location of topographic swath profiles A–E (width of sampling corridor is 20 km) between the Alpine fault and the main divide of the Southern Alps. Thick black and thin grey lines indicate mean, and ± 1 S.D. from the mean of elevation (m a.s.1.) and slope (°) within each swath, respectively. Note varying scale on *x*- and *y*-axes. Shown on left are inferred dip-slip rates along the Alpine fault, dipping at ≥5° (Norris and Cooper, 2000).

the whole width of the study area to obtain a more regional picture.

To obtain a measure for local relief, we used both kernel- and surface interpolation methods. The kernel-based method we chose computes the standard deviation of elevation within a moving sampling window (circle) for a range of sampling radii *R*. This neighbourhood statistical method is objective, though rather insensitive to differences in valley spacing and orientation. We therefore also extracted point elevation data along the major catchment divides and interpolated from them surfaces to obtain the sub-ridgeline relief (Brocklehurst and Whipple, 2002). We do not expect that such interpolated surfaces have existed as real geomorphic surfaces at any time in the past. Their only geomorphic significance here is that they provide a rough means to indicate the volume "missing", i.e. presumably eroded, beneath major drainage divides. This assumption does not include the possibility of structural basins. Interpolation routines for the point data used were (a) the inverse distance weighted (IRW) method with a variable search radius; (b) tension spline; and (c) ordinary kriging, also with variable search radius. To test the accuracy of these regional interpolations, we also extracted profile data for 30 valley cross-sections perpendicular to major river channels, where tributary influence was minor.

4. Regional-scale analysis of the relief of the western Southern Alps

4.1. Elevation and relief

Elevation in the WSA ranges from ~10 m a.s.1. (Arawhata) to nearly 3490 m a.s.1. (Fox) over a horizontal distance between the Alpine fault and the main divide. The highest peak in the Southern Alps, Mt Cook (3754 m a.s.l.), is located a few kilometers to the E of the main divide. Elevation distribution is Gaussian with a mean at 1082 m a.s.1.

Topographic swath profiles between the Alpine fault and the main divide show the influence of major oblique and longitudinal valleys such as the Arawhata and Landsborough, respectively (Fig. 3C, E). In contrast, where elevations are highest around the nevees of Franz Josef and Fox Glacier, west of Mt Cook, the increase in elevation away from the Alpine fault is less irregular (Fig. 3B). Mean elevation also shows a steep increase along the first 2 km adjacent to the Alpine fault (Fig. 3B, C, D), although data need to be interpreted with care, since the fault truncates hillslopes of the range front north of Haast, whereas much of its trace south of Haast is located immediately west of the range front. Regionally, mean elevation declines SW-ward from 1583 m

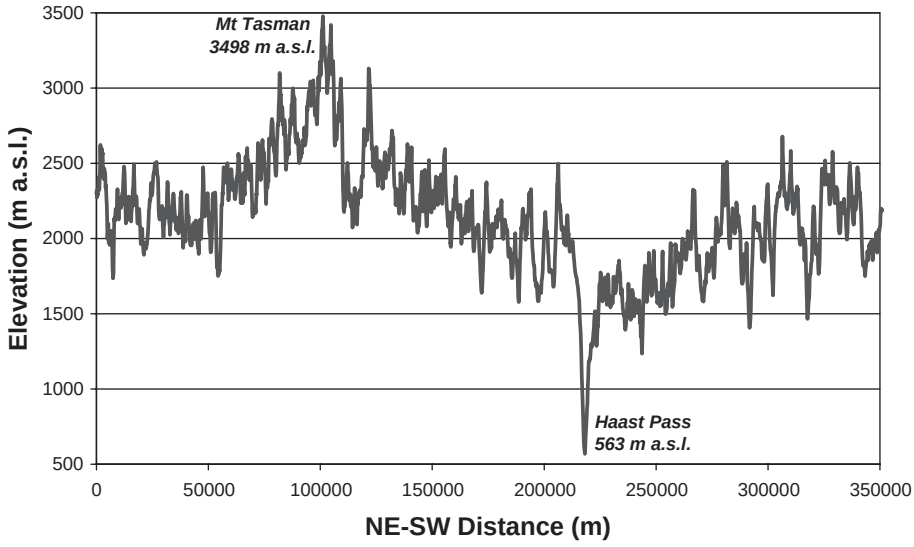

Fig. 4. Elevation profile of the main divide of the Southern Alps in the study area, which does not include New Zealand's highest peak (Mt Cook, 3574 m a.s.1.). Haast Pass has been a site of glacial transfluence repeatedly during glacial maxima.

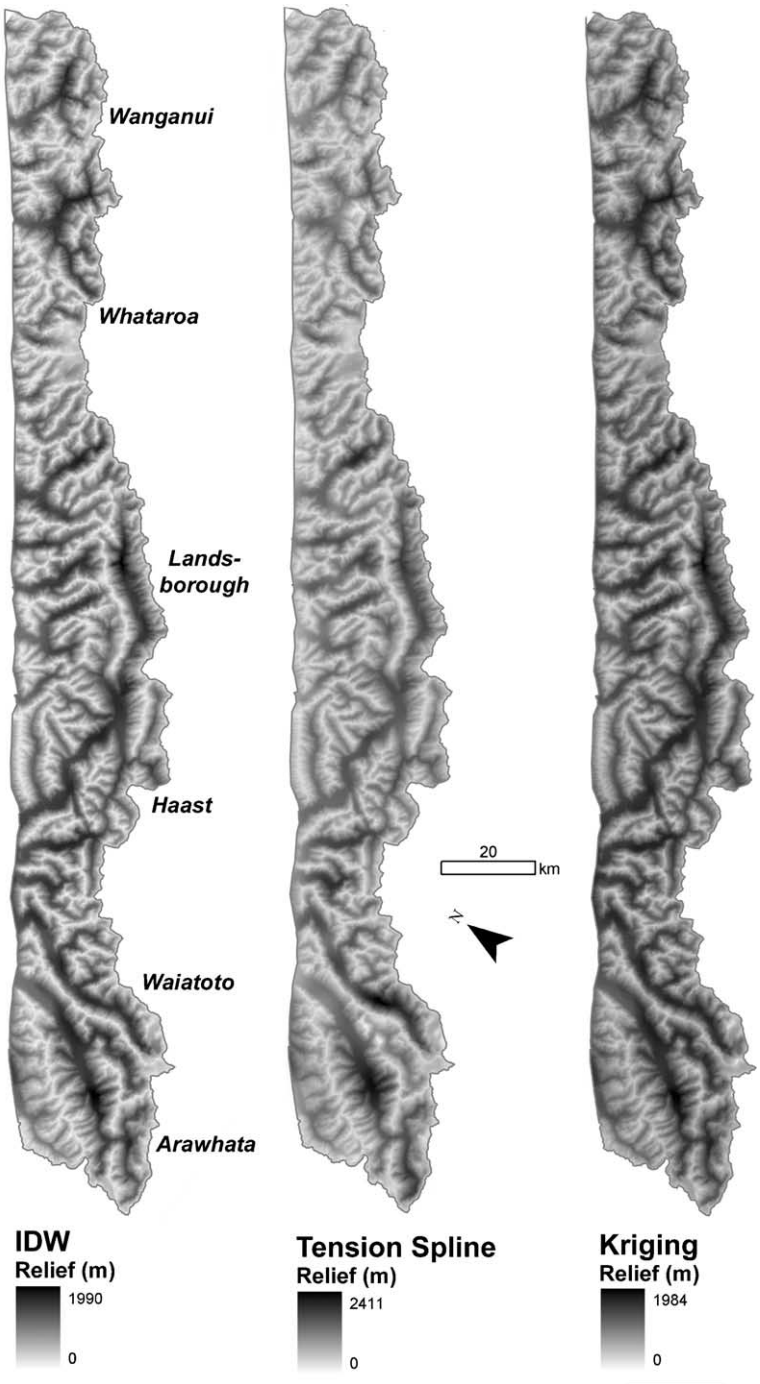

Fig. 5. Mean basin relief for the WSA. Relief was derived from subtraction of present topography from surfaces based on elevation points along major catchment divides. See text for explanation.

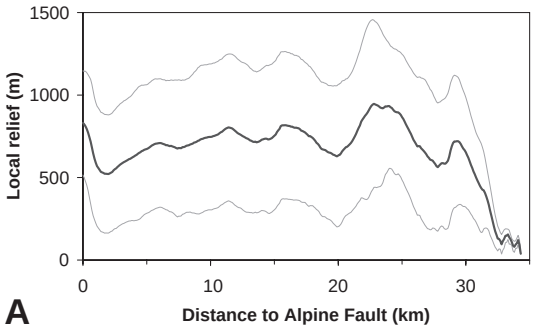

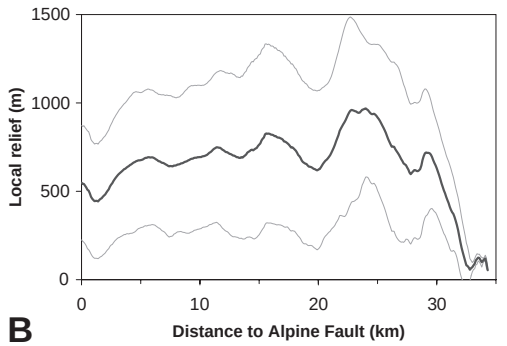

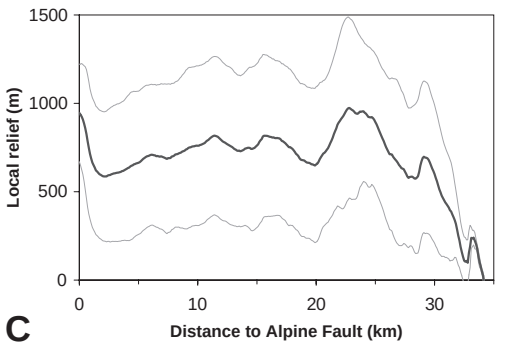

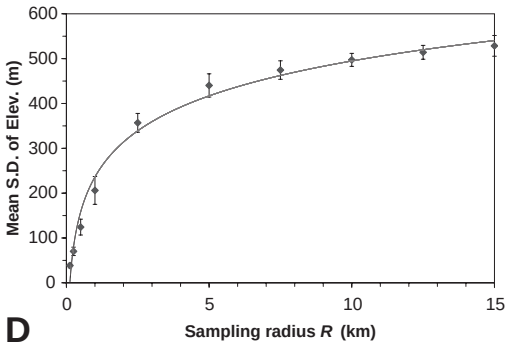

Fig. 6. Swath profiles of mean basin relief of the WSA between the Alpine fault and main divide, derived from Fig. 5. Mean basin relief was computed as the elevation difference between interpolation surfaces between major catchment divides and the present topography, using A: inverse distance weighted (IDW) method; B: tension spline, and C: ordinary kriging. Regional-scale differences between these models are minute. Local relief is highest at ~22 km SE of the Alpine fault; start and end points of the swath profiles show calculation artefacts. Thick black and thin grey lines indicate mean, and ±S.D. from the mean of elevation within each swath, respectively. D: Decrease of S.D. of elevation in the WSA with increasing sampling radius R for a moving circle window. Note that $R>10$ km already leads to boundary effects due to the narrowness of the orogen.

a.s.1. (swath profile B) to 1056 m a.s.1. (swath profile E).

The main divide has a length of 353 km in the study area, attaining elevations between 563 m a.s.1. (Haast Pass) and 3498 m a.s.1. (Mt Tasman), with a mean of 2143 m a.s.1. (Fig. 4). Its distance to the Alpine fault is minimal (14 km), where it is highest, although it is generally <2500 m a.s.1. SW of Haast Pass, where it defines another NW-ward arc.

The sub-ridgeline relief in the WSA varies slightly by spatial pattern and quantity, depending on the type of interpolation method (Fig. 5). The results of the IDW and the kriging method do not differ considerably, whereas the tension spline method produced larger values of local relief on average. Depending on the interpolation method, local relief in the WSA has an average of 0.65–0.68 km. All three methods yield similar spatial patterns of high local relief (>1.5 km), which attain ~2 km in the middle Arawhata and Waiatoto valleys, the upper Landsborough, the Haast, Whataroa, and others. Average relief is highest (0.95 km) at ~22 km distance from the Alpine fault (Fig. 6), showing a clear influence by major longitudinal valleys.

By subtracting the DEM from the interpolated sub-ridgeline surface, we obtain rough estimates of the volumes of rock V^* "missing" below the catchment divides from each major valley. Such volumes are by all means only first-order indications of erosion, since they do not include any erosion or shifting of catchment divides. For instance, the Arawhata catchment, which features some of the highest relief in the WSA, may have lost 625–633 km^3 to erosion below its divides, depending on the interpolation method (Table 2). V^* shows a strong ($R^2=0.98$) power–law relationship with catchment area A (slope $\beta=1.13$;

Table 2
Inferred volumes of "missing" rock from below major catchment divides

Catchment	Area (km^2)	Inferred volume ''missing'' (km^3)			Mean basin relief (km)		
		IDW	Tension spline	Ordinary kriging	IDW	Tension spline	Ordinary kriging
Waitaha	134.0	68	71	68	0.51	0.53	0.51
Wanganui	342.7	221	194	234	0.64	0.57	0.68
Poema	63.9	36	35	37	0.56	0.55	0.58
Whataroa	452.9	340	288	348	0.75	0.64	0.77
Waiho	163.8	90	83	94	0.55	0.51	0.57
Fox	91.6	47	49	48	0.51	0.53	0.52
Cook	130.7	79	75	84	0.60	0.57	0.64
Karangarua	361.0	267	251	276	0.74	0.70	0.76
Makawhio	114.0	79	82	79	0.69	0.72	0.69
Mahitahi	153.1	128	121	130	0.84	0.79	0.85
Paringa	225.8	163	155	168	0.72	0.69	0.74
Moeraki	62.4	42	36	43	0.67	0.58	0.69
Haast	1313.2	1018	1013	1040	0.78	0.77	0.79
Turnbull	147.3	109	124	107	0.74	0.84	0.73
Okuru	214.8	168	158	171	0.78	0.74	0.80
Waiatoto	441.7	350	366	355	0.79	0.83	0.80
Arawhata	757.3	625	626	633	0.83	0.83	0.84

Volumes were calculated by subtracting the DEM from interpolated surfaces of sub-ridgeline relief, using inverse distance weighted method (IDW), tension spline, and ordinary kriging. Mean basin relief was calculated by normalizing "missing" volume by catchment area.

intercept $k=0.35$; $p<0.01$). A more physically significant meaning is obtained, when normalizing V^* by A. The resulting mean basin relief is an integral measure of the average elevation difference between ridgelines and the channel for a given basin. It ranges between 0.51 and 0.85 km, with a mean of 0.69 km.

We also chose the standard deviation of elevation within radius R as a suitable measure of local relief variability. At sufficiently high R, we expect to objectively record local relief irrespective of catchment divides or other topographic constraints. In the WSA, this values appears to be ± 0.5 km for $R=10$ km (Fig. 6D), which we see as a critical sampling length, above which boundary effects due to the narrow orogen width (~20–35 km) distort our results.

Profiling data from individual valley cross-sections show comparable results, asserting maximum local relief of >2 km roughly halfway between Alpine fault and main divide (Fig. 7). Valley cross-sectional areas, calculated beneath a straight line linking the highest points of each profile, are positively correlated with contributing catchment area, regardless of v- or u-shaped cross-sections (Fig. 7A). The same applies for local relief, which was measured as the elevation difference between the average of the highest divide points and the thalweg. Maximum divide spacing appears to be less influenced by contributing catchment area (Fig. 7B, C).

4.2. Hypsometry

Hypsometric integrals for the 22 study catchments show an inverse correlation with catchment area and are thus scale dependent (Fig. 8). The nature and degree of correlation changes with catchment area. A sample of 32 sub basins ($A<50$ km^2) of the Whataroa catchment shows a contrasting positive linear relationship and a broader range of values. Hypsometric integrals for major catchments are exclusively <0.5.

Hypsometric curves of presently strongly glaciated basins (Waiho, Fox) show a distinct convexity, which however differs not much from some larger basins presently dominated by fluvial processes such as Waitaha or Wanganui Rivers (Fig. 9A). Basin size exerts some effect on the shape of hypsometric curves, with some of the larger basins showing lesser normalized elevation for a given area (Fig. 9B). Moreover, moderately glaciated basins such as that

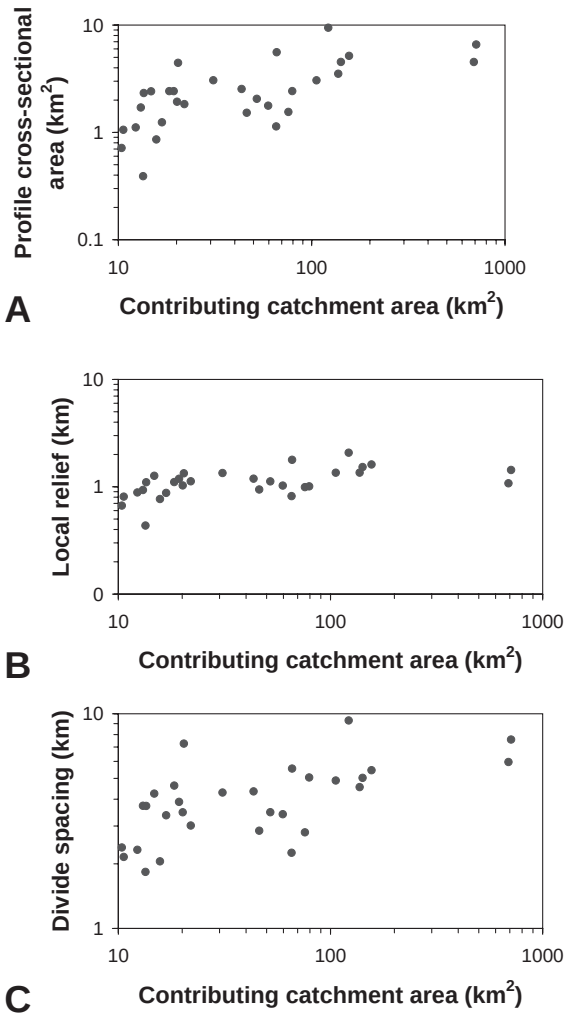

Fig. 7. A. Cross-sectional area; B. local relief; and C. maximum divide spacing, as a function of contributing catchment area for 30 valley cross-sections in the WSA (see Fig. 12 for location).

of Cook River, which features several valley glaciers, may not stand out as such, when compared to other fluvial dominated basins (Fig. 9C).

4.3. Gradient

The modal, i.e. most frequent, slope (φ) in the WSA is 38–40°. Given the resolution of the DEM, we anticipate that these gradients are underestimates of real values (Finlayson and Montgomery, 2003). Bimodality in slope-angle distributions occurs in catchments with extensive glacier cover and valley fills. The spatial pattern of mean slope (ψ), which is 30° in the WSA, is somewhat uniform from NW to SE. Values of ψ for individual swath profiles A–D are 32–33°, but only 27° for profile E.

The profiles show the local lowering effect on slope angles of extensive ice cover (Fig. 3B) and major longitudinal and oblique valleys (Fig. 3C, E). Elsewhere, ψ remains somewhat constant across the width of the WSA (Fig. 3A, D). The swath profiles also highlight the non-linear relationship between ψ and mean elevation in the WSA. To explore any vertical patterns of slope distribution, we plotted the variation of mean and modal slope angles as a function of 200-m elevation bins (Kühni and Pfiffner, 2001) for catchments NE and SW of Haast (Fig. 10). We chose to split the data at Haast because of the significantly decreasing dip-slip rates on the Alpine fault SW of Haast (Norris and Cooper, 2000). These plots also demonstrate the non-linear relationship between slope and elevation in the WSA. However, we are able to differentiate between four altitudinal domains for catchments NE of Haast (Fig. 10A):

(i) low-altitude (l0–400 m a.s.1.) areas with the lowest ψ;
(ii) montane to subalpine (400–l800 m a.s.1.) areas with a remarkably constant φ of 38–40° and a linear increase of ψ with elevation;
(iii) alpine (1800–2600 m a.s.1.) areas in which both ψ and φ significantly fall below those of the montane zone; and
(iv) high alpine (2600–3400 m a.s.1.) areas with some of the highest mean and modal slope angles (>45°) in the WSA.

A similar pattern is observed in catchments SW of Haast (Fig. 10B), where the difference between mean and modal slope angles is higher above 2200 m a.s.l., and less at 1600–2200 m a.s.1. For the whole of the WSA, slope angles exhibit a conspicuous linear increase with elevation between 300 and 1300 m a.s.1.

4.4. Rivers

River longitudinal profiles of major alpine rivers in the WSA have both concave and convex, irregular,

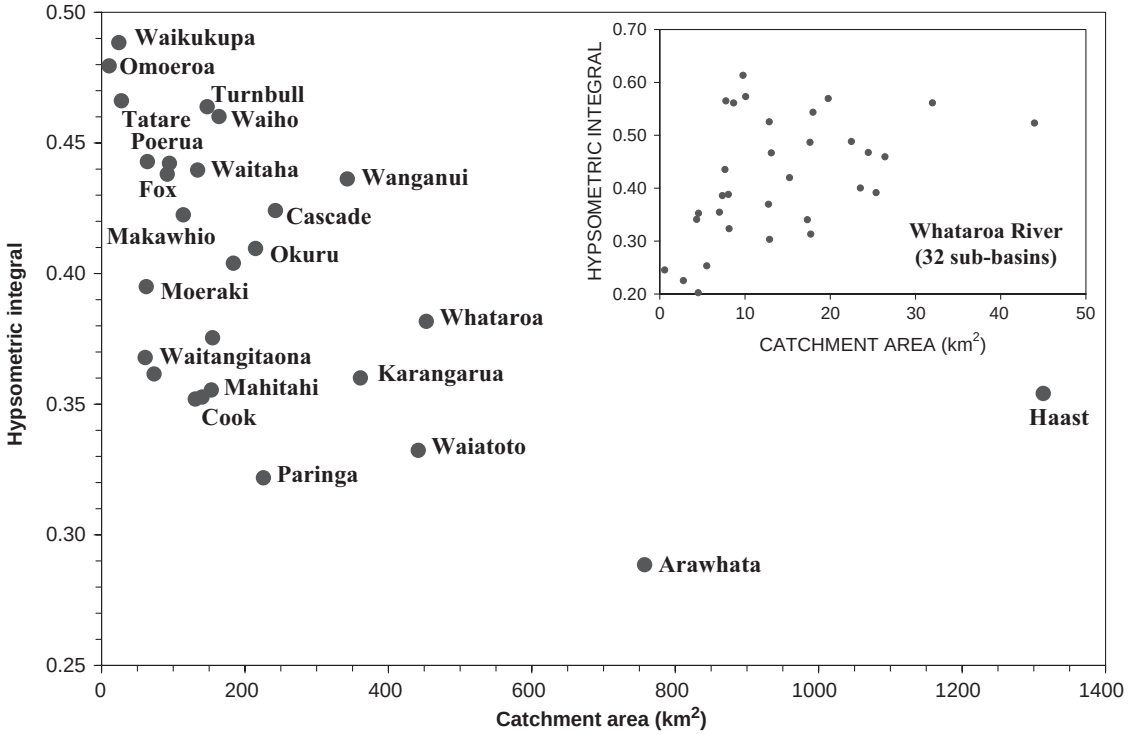

Fig. 8. Hypsometric integrals versus catchment areas for major catchments in the WSA. Inset shows hypsometric integrals of 32 watersheds in the Whataroa basin.

and stepped profiles (Fig. 11), and there are 131 major waterfalls in the study area. Glacial scour is locally evident in cirques and stepped bedrock profiles with prominent knickpoints such as on Staircase Creek, on the Okuru River (Fig. 11C). Numerous oversteepened reaches occur at tributary junctions. The intense fluvial slope dissection with drainage densities of ~50 km km^{-2} (Basher et al., 1988) is however insufficiently resolved in the DEM.

To obtain a regional overview of fluvial erosion potential in the WSA, we adapted the method of Finlayson et al. (2002) and modelled specific stream power for major rivers (Eq. (2)). McKerchar and Pearson (1989) showed that catchment area A is a good proxy for the mean annual flood Q_f in the WSA

$$Q_f = 15A^{0.808} \quad (3)$$

They also noted that floods with 1% annual exceedance probability had a discharge varying only by a factor of 1.8–2 from Q_f. We therefore assume that use of a specific stream-power model

$$\varepsilon = A^{0.5}S \quad (4)$$

for regional-scale modelling of fluvial erosional potential, despite its simplicity, will cover a wide range of realistic flood discharges. Modelling results for trunk channels in the WSA, arbitrarily defined here as having $A \geq 10$ km^2, show highest inferred erosion rates (normalized for maximum values) in reaches dominated by steep bedrock gorges, especially those in the Whataroa, Landsborough, and Arawhata catchments (Fig. 12).

Nearly 50% of the fluvial terraces we sampled from the DEM are located <40 m above the channel floor (Fig. 13A). Exceptional remnant surfaces in the lower Waitaha River have relative heights of ~320 m. No significant high-level fluvial terraces were detected from the DEM SW of Haast, where broad valley trains with low-angle tributary fans dominate.

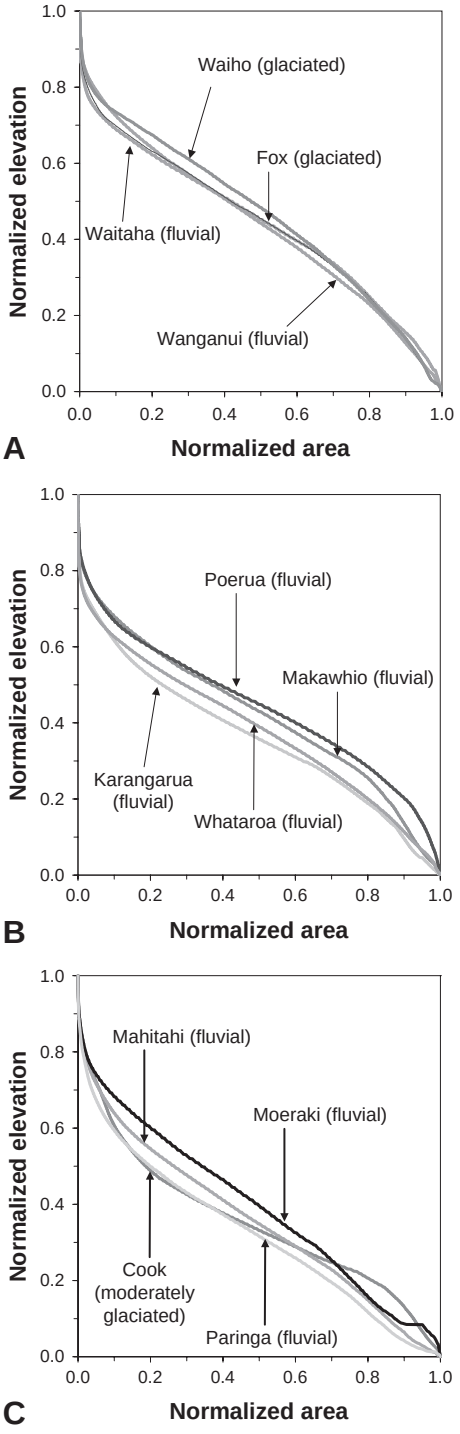

The distance from the Alpine fault however appears to be have little influence on the terrace elevations as a whole. Similarly, data on elevation of knickpoints are also devoid of any conclusive distribution with respect to their downstream flow distance from the Alpine fault (Fig. 13B).

5. Discussion

The relief of the WSA is the result of high rates of rock uplift and surface processes. This interaction has created deeply incised valleys, with local relief attaining ~2 km in the upper to central parts of major catchments, at several kilometers distance from both the Alpine fault and main divide (Figs. 5 and 6). Standard deviation of elevation within a 10-km radius is $\pm$0.5 km, and an objective measure of mean regional relief variability. Major longitudinal valleys such as the Landsborough significantly add to relief production in the WSA although this particular valley was added to the westward drainage by stream piracy (Craw et al., 2003). Although valley cross-sectional area, local relief, and divide spacing generally increase with contributing catchment area A (Fig. 7), these values do not peak at the Alpine fault, where A is at a maximum. This is because mean elevation decreases towards the range front, thereby reducing the overall potential for high relief.

Hypsometric integrals in the WSA show contrasting relationships with catchment area (Fig. 8). In accordance with Hurtrez et al. (1999), we caution their use for regional analysis of mountain terrain. Similar to the findings of Bishop et al. (2002) for the Nanga Parbat area, Pakistan, we observe that, for the majority of basins, the shapes of hypsometric curves alone do not allow a clear distinction between glacial or fluvial dominance without other information (Fig. 9).

Swath profiling shows that, in the WSA, mean slope angle ψ is lowered where major longitudinal

Fig. 9. Hypsometric curves for selected catchments in the WSA. A. Note the similar shape of curves for basins with high (Waiho, Fox) and low degree of contemporary ice cover (Waitaha, Wanganui). B. Influence of catchment area (large for Karangarua and Whataroa) on hypsometric curve. C. Partial similarity of curves for moderately glaciated (Cook) and fluvial dominated basins.

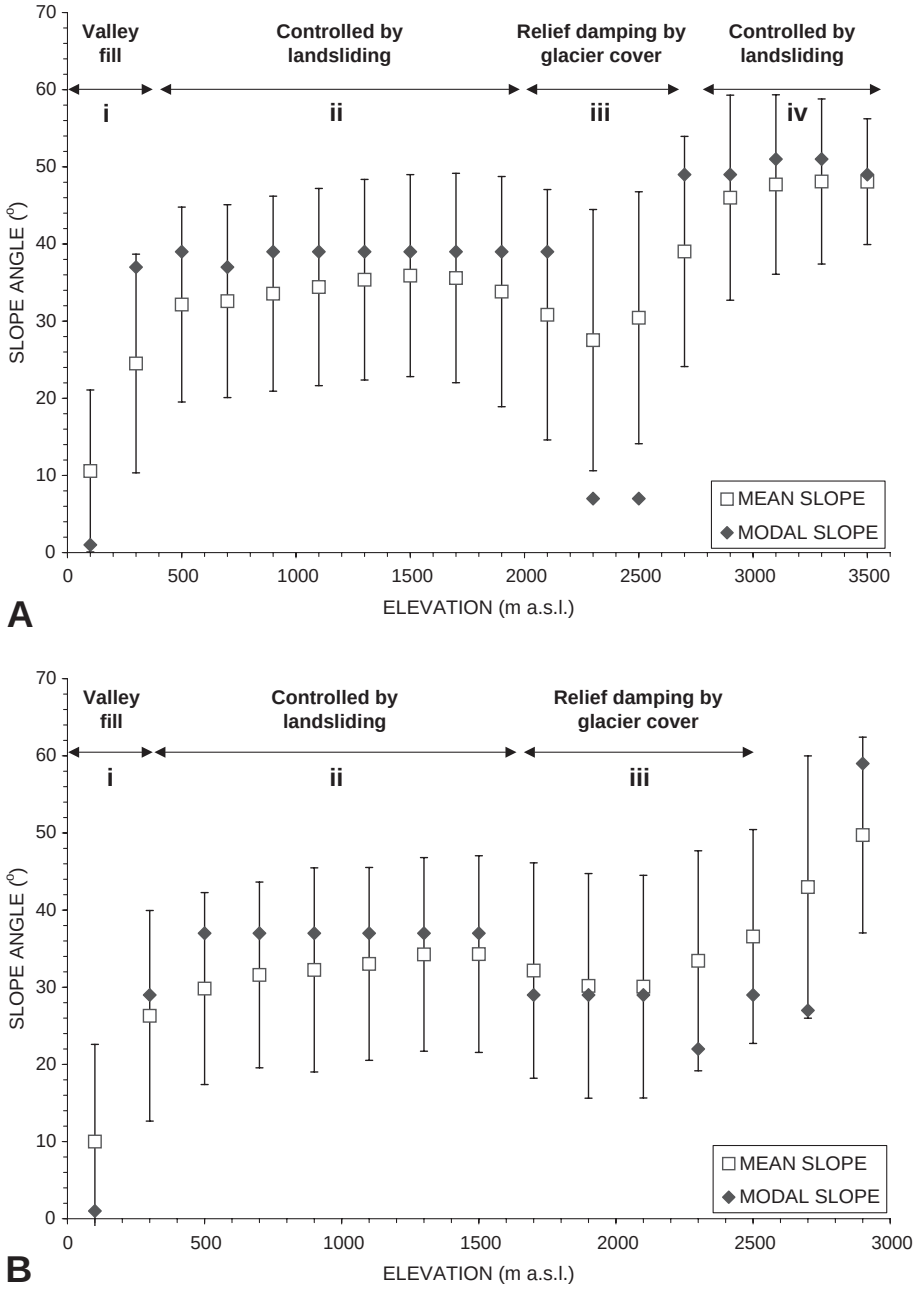

Fig. 10. Mean and modal slope angle as a function of 200-m elevation bins for A. catchments NE of Haast, and B. catchments SW of Haast. Four domains have been differentiated and attributed to dominant geomorphic processes.

valleys and extensive ice cover occur (Fig. 3). Some swath profiles demonstrate that ψ is an insensitive measure for highlighting regional variations (Fig. 3D). Several studies in other mountain belts have demonstrated the independence of regional slope angle distributions from denudation rates, and have inferred the presence of fluvial incision-driven threshold slopes, or climatic forcing on relief (e.g., Burbank

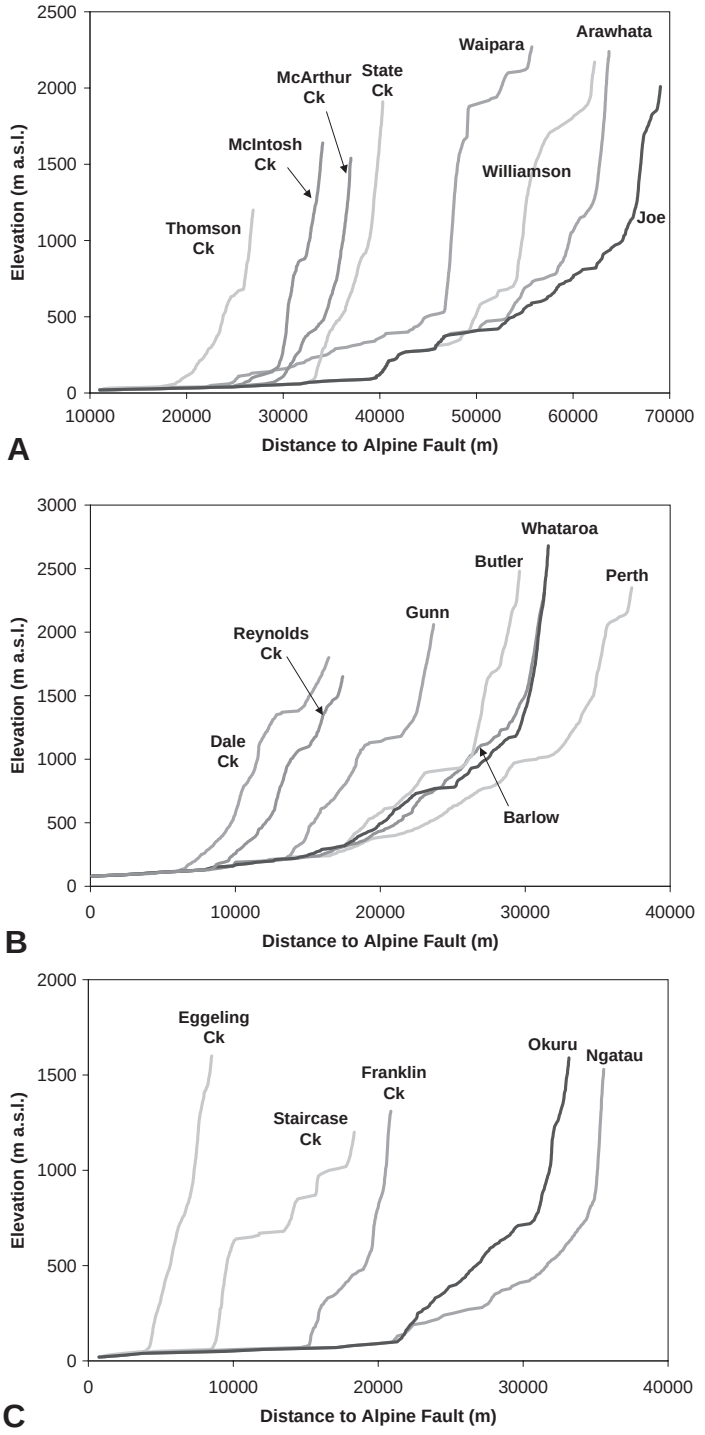

Fig. 11. Selected longitudinal profiles of rivers in the WSA. A. Arawhata, B. Whataroa, and C. Okuru Rivers (black), and major tributaries (grey shades). Note prevalence of knickpoints and stepped profiles (e.g., Staircase Ck, Okuru).

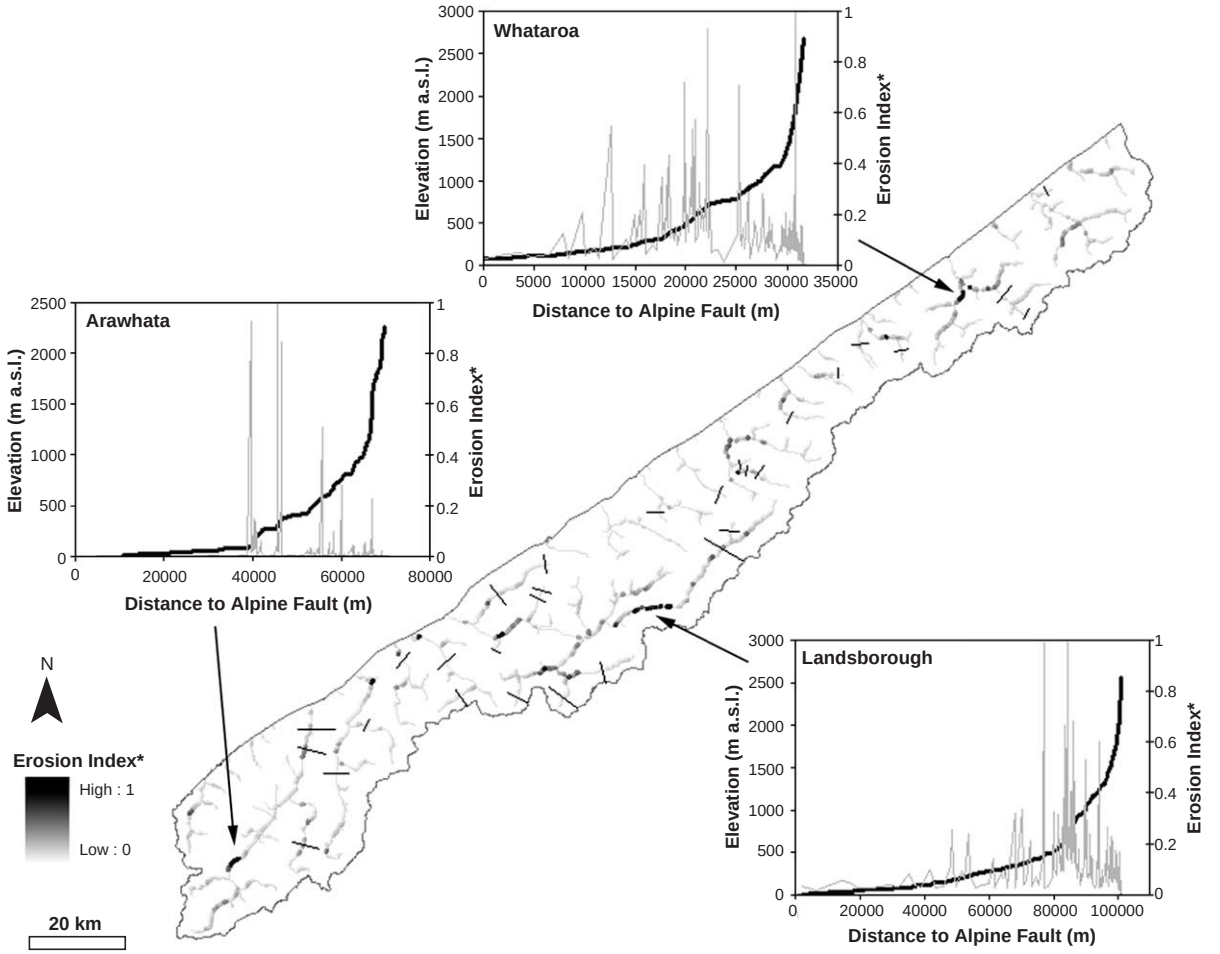

Fig. 12. Results from regional modeliing of erosion index $\varepsilon = A^{0.5} S$ (Finlayson et al., 2002) for major trunk channels ($A \geq 10$ km^2) in the WSA. Erosion index was normalized against highest values in the respective catchments (standing out as black dots along the channels), and shows spatial coincidence with steep bedrock gorges. Diagrams depict river longitudinal profiles (black) and local variability of ε (grey). Black lines on map denote locations of valley cross-sections (see Fig. 7).

et al., 1996; Brozovic et al., 1997; Montgomery, 2001; Gabet et al., 2004).

The non-linear relationships between slope and elevation (Fig. 10) may be interpreted on the basis of dominant geomorphic processes (e.g., Whitehouse, 1988) in four altitudinal domains: (i) Low-altitude (0–400 m a.s.l.) areas have the lowest ψ, and correspond to major valley trains and low-angle alluvial fans dominated by fluvial processes. (ii) Montane to subalpine (400–1800 m a.s.l.) slopes show a remarkably constant $\varphi = 38$–40°, while ψ increases linearly with elevation. Surface runoff and frequent landsliding are dominant geomorphic agents in this domain. We note that φ may record some hillslope adjustment process to frequent erosion and closely coupled fluvial incision. Locally, it may also reflect the bedrock angle of repose or dip of schistosity, since we observe that landsliding on ridges flanking glaciers and ice fields produces much steeper slopes. (iii) In alpine (1800–2600 m a.s.l.) areas both ψ and φ are significantly below those of the montane zone. We attribute this to the "relief dampening" effect of ice cover, i.e. glacier slopes characterized by slopes $<30^\circ$. (iv) High-alpine (2600–3400 m a.s.l.) areas of bare rock have the highest mean and modal slope angles ($>45^\circ$) in the WSA. Judging from its elevation and slope character-

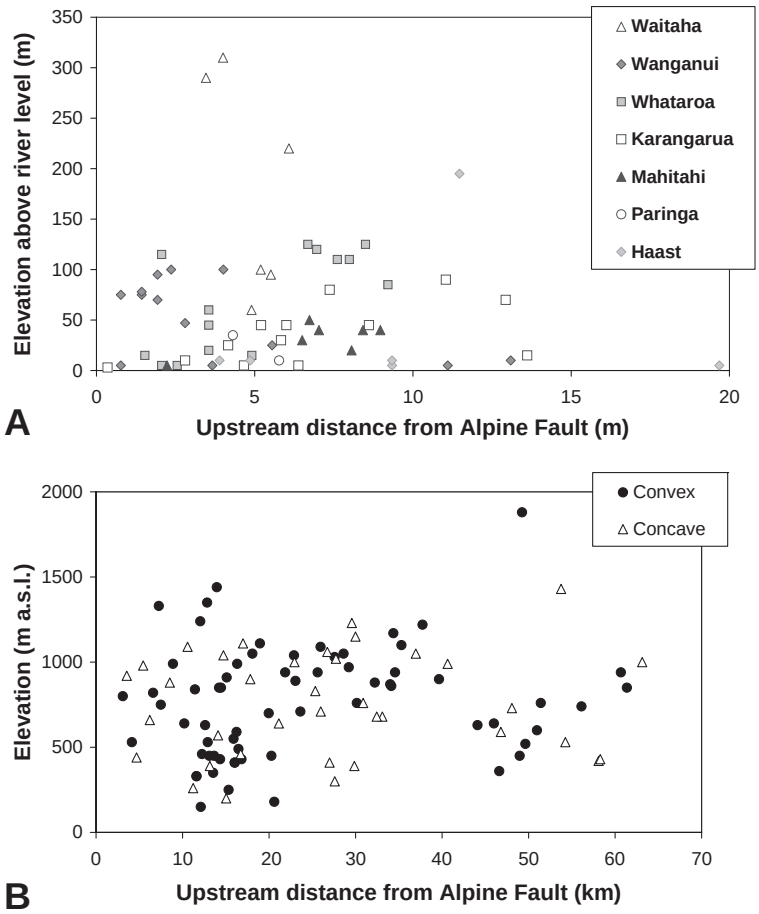

Fig. 13. A. Elevation of erosional and aggradation terrace tread levels (±3 m vertical accuracy) as a function of distance from Alpine fault. B. Elevation and distance from Alpine fault of major concave and convex knickpoints derived from river longitudinal profiles.

istics, we interpret this domain to constitute much of the main divide, and be shaped by rock fall/rock avalanching (McSaveney, 2002).

Due to limited geological data coverage, our analysis of slope angles did not include structural influence on the relief of the WSA, which appears to control much of the orientation of low-order drainage in particular. Schistosity planes and faults also locally control slope relief, forming rectilinear dip-slopes and rock-slope buttresses, while promoting large-scale gravitational collapse (Craw et al., 2003; Korup, 2005b).

Regional modelling of specific stream power suggest that the highest potential for fluvial incision is in reaches occupied by steep bedrock gorges and associated knickpoints in the mid-reaches of major catchments (Fig. 12). These focal points of high inferred erosion adjoin zones where the sub-ridgeline relief is inferred to be highest in the WSA, i.e. 10^3 km^3 of "missing" volume, or >0.8 km of mean basin relief (Fig. 5; Table 2). We note that the modelled focal points of fluvial erosion do not fully coincide with the highest local relief. Many of the bedrock gorges, where river incision supposedly is the highest in the mountain belt, extend over several hundreds of vertical meters, and thus affect the computation of local relief.

The distribution of terrace treads and major knickpoints with regard to their distance from the Alpine fault shows significant scatter (Fig. 13). We interpret the lack of any obvious trend in the terrace data as the

superposition of local controls such as sediment supply, tributary-trunk adjustments, or glacial pre-design, on any potential tectonic signal of base-level lowering. Some of the flat surfaces at high elevations may also be infilled ponds or remnants of uplifted marine terraces (Bull and Cooper, 1986). Historic landslides produced >10-m thick aggradation surfaces in high-energy bedrock gorges in the WSA (Korup et al., 2004). Thus we do not expect any necessity for a regional correlation of terrace levels with coseismic uplift. Adams (1980) argued that warping of major terraces in the Wanganui and Whataroa basins occurred in response to drag movement SE of the Alpine fault. DEM data show no such trends, yet depict a general decrease of notable high-level terraces towards the south. Their absence SW of Haast coincides with low local uplift rates (<2 mm y^{-1}; Norris and Cooper, 2000).

Average river incision rates locally attain 0.5–58 mm y^{-1}, averaging 11 ± 4 mm y^{-1}, based on ^{14}C-

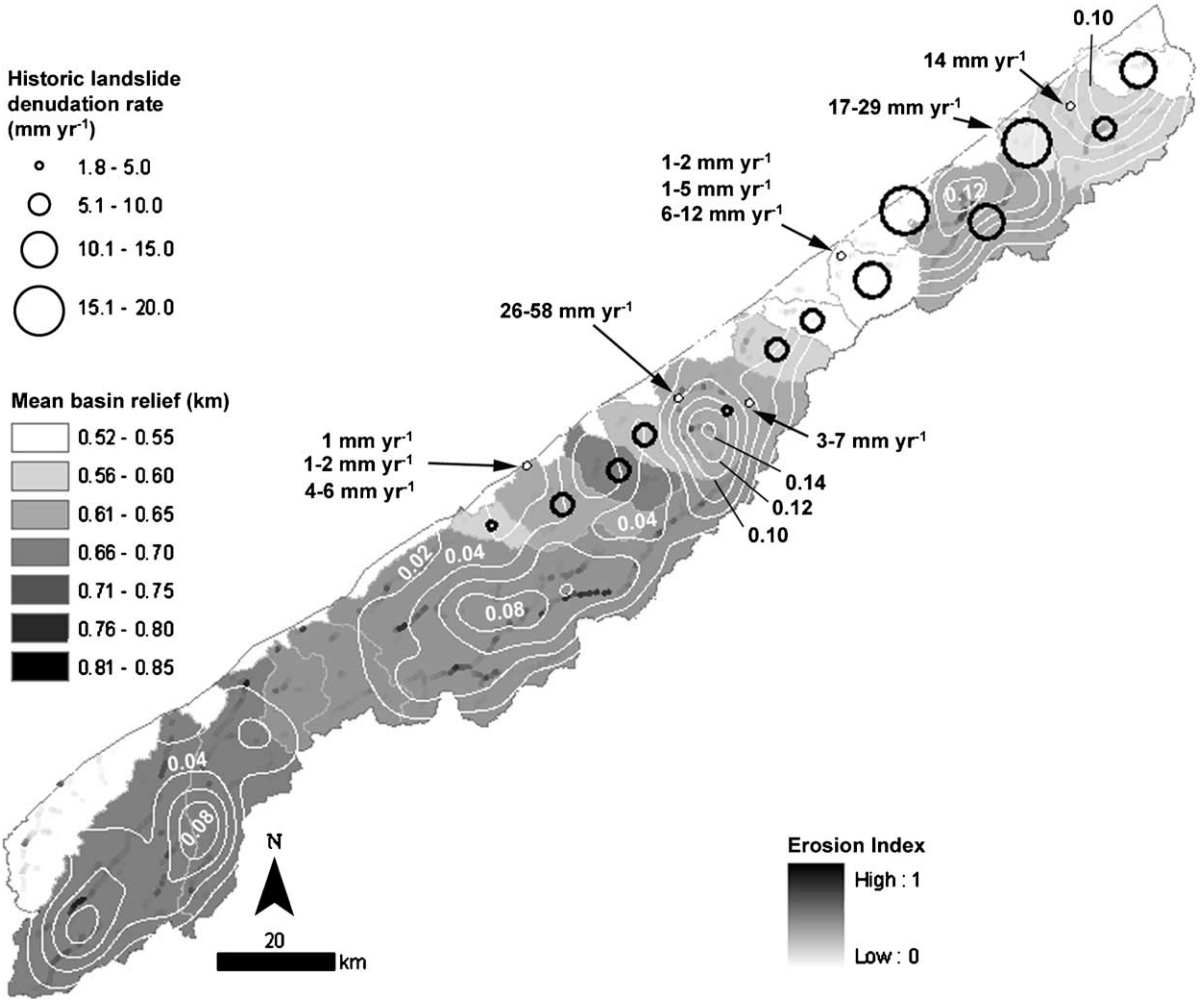

Fig. 14. Summary of erosion and denudation data for the WSA. Mean basin relief was calculated by normalizing inferred eroded rock volume below major divides by catchment area, using the mean of interpolation methods in Fig. 5 and Table 2. Circles denote denudation rates from historic landslides <1 km^2 in the montane zone NE of Haast River (Hovius et al., 1997). Contours show landslide density [km^{-2}] calculated from inventory data (Korup, 2005a). Erosion index for fluvial bedrock incision rates taken from Fig. 12. Arrowed white points show river incision rates inferred from ^{14}C-dated fill terraces (see text for sources), which likely overestimate long-term bedrock incision.

dates from ten sites between the Wanganui and Paringa Rivers (Adams, 1980; Simpson et al., 1994; Yetton et al., 1998; Burrows et al., 2002; Fig. 14). Since these rates were derived from fill terraces, they most likely overestimate long-term bedrock incision rates. If we assume a conservative uplift rate of 5 mm y^{-1}, some of the high-level (~100-m) terraces recorded in the DEM may indeed represent postglacial aggradation surfaces such as the ones dated by Adams (1980). Further detailed field investigations will be necessary to ascertain erosional or depositional formation for major terraces. The study on aggradation terraces has important implications for hazard and risk assessments in the WSA, where there is currently a high and increasing probability for a M ~8 earthquake on the Alpine fault (Wells et al., 1999). Widespread coseismic landsliding brings the potential for considerable aggradation of rivers with landslide debris (Yetton et al., 1998). If such sedimentary evidence for former rupture events were preserved in the valley trains of the WSA, detailed studies could reconstruct the volumes of sediment likely to be mobilized following future high-magnitude earthquakes.

In summary, data on mean basin relief and stream-power erosion index, together with the average fluvial incision rates mentioned above, historic landslide denudation rates (Hovius et al., 1997), and landslide density [km^{-2}] calculated from a regional inventory (Korup, 2005a), give a first regional overview of erosion and denudation rates and their relationship to relief in the WSA (Fig. 14).

6. Conclusions

We have compiled a preliminary map of regional erosion and denudation by overlaying mean basin relief, a modelled stream-power erosion index, river incision rates, historic landslide denudation rates (Hovius et al., 1997), and landslide density (Korup, 2005a). The interplay between strong tectonic and climatic forcing in the WSA has led to relief production that locally attains ~2 km, with a SW-ward decrease of mean elevation by 500 m between Waiho and Arawhata Rivers. Local relief and inferred river bedrock incision rates are highest about half-way to two-third of the distance between the Alpine fault and the main divide. Mean local relief peaks at 0.95 km, at ~22 km distance from the Alpine fault, showing clear influence by major longitudinal valleys. Depending on the interpolation method, local relief has an average of 0.65–0.68 km. Local relief, valley cross-sectional area, and divide spacing correlate moderately with catchment area, and also peak between the range front and the divide. The inferred volume of eroded rock beneath major catchment divides ranges between 10^1 and 10^3 km^3 and is strongly dependent on catchment area. For the larger basins ($A > 60$ km^2), this translates into a mean basin relief of 0.51–0.85 km. The mean basin relief of 0.69 km corresponds well with the local relief. The elevation of the main divide shows no relationship to its distance from the Alpine fault.

Hypsometric integrals correlate with catchment area, and together with hypsometric curves, proved ambiguous for differentiating between glacial and fluvial dominated basins without any prior knowledge. Mean slope angle ($\psi = 30^\circ$) is lowered where major longitudinal valleys and extensive ice cover occurs, and may be an insensitive measure of regional relief rather than be independent of endogenic and exogenic controls. Modal slope angle is strikingly uniform throughout the WSA ($\varphi = 38$–40°), and may record some adjustment process to surface runoff and frequent landsliding. Both ψ and φ show a non-linear relationship with elevation, which we attribute to the result of dominant geomorphic process domains, such as fluvial processes in low-altitude valley trains, surface runoff and frequent landsliding on montane hillslopes, "relief dampening" by glaciers, and rock fall/avalanching on steep main divide slopes.

River longitudinal profiles show a variety of forms ranging from dominantly concave to convex. Remnants of glacial erosion are evident in cirques, rock steps and basins, and steep gorges. Quantitative analyses of river longitudinal profiles may be a future working step to providing further insights into the regional variation of their steepness and concavities (e.g., Kobor and Roering, 2004). The same applies to better quantification and mapping of differential uplift and erosion in the WSA, in order to compare the findings of our regional-scale analysis with relief-shaping processes over a range of time scales.

Acknowledgements

We thank E.M. Keller, A.M. Harvey, and an anonymous referee for their comments on an earlier manuscript.

References

Adams, J., 1980. Palaeoseismicity of the Alpine fault seismic gap, New Zealand. Geology 8, 72–76.

Augustinus, P.C., 1992. The influence of rock mass strength on glacial valley cross-profile morphometry: a case study from the Southern Alps, New Zealand. Earth Surface Processes and Landforms 17, 39–51.

Baillie, I.C., Norbu, C., 2004. Climate and other factors in the development of river and interfluve profiles in Bhutan, Eastern Himalayas. Journal of Asian Earth Sciences 22, 539–553.

Basher, L.R., Tonkin, P.J., McSaveney, M.J., 1988. Geomorphic history of a rapidly uplifting area on a compressional plate boundary: Cropp River, New Zealand. Zeitschrift für Geomorphologie, Supplementband NF 69, 117–131.

Batt, G.E., Braun, J., 1999. The tectonic evolution of the Southern Alps, New Zealand: insights from fully thermally coupled dynamical modelling. Geophysical Journal International 136, 403–420.

Bishop, M.P., Shroder Jr., J.F., Bonk, R., Olsenholler, J., 2002. Geomorphic change in high mountains: a western Himalayan perspective. Global and Planetary Change 32, 311–329.

Bishop, M.P., Shroder Jr., J.F., Colby, J.D., 2003. Remote sensing and geomorphometry for studying relief production in high mountains. Geomorphology 55, 345–361.

Brabyn, L., 1997. Classification of macro landforms using GIS. ITC Journal 1, 26–40.

Brocklehurst, S.H., Whipple, K.X., 2002. Glacial erosion and relief production in the Eastern Sierra Nevada, California. Geomorphology 42, 1–24.

Brocklehurst, S.H., Whipple, K.X., 2004. Hypsometry of glaciated landscapes. Earth Surface Processes and Landforms 29, 907–926.

Brozovic, N., Burbank, D.W., Meigs, A.J., 1997. Climatic limits on landscape development in the northwestern Himalaya. Science 276, 571–574.

Bull, W.B., Cooper, A.F., 1986. Uplifted marine terraces along the Alpine Fault, New Zealand. Science 234, 1225–1228.

Burbank, D.W., Leland, J., Fielding, E., Anderson, R.S., Brozovic, N., Reid, M.R., Duncan, C., 1996. Bedrock incision, rock uplift, and threshold hillslopes in the northwestern Himalaya. Nature 379, 505–510.

Burrows, C.J., Bell, D., Grant, H., 2002. Two new radiocarbon ages for mid- and late-Aranui age valley-train deposits of the Franz Josef Glacier, Westland, New Zealand. Journal of The Royal Society of New Zealand 32, 415–425.

Craw, D., Nelson, E., Koons, P.O., 2003. Structure and topographic evolution of the Main Divide in the Landsborough–Hopkins area of the Southern Alps, New Zealand. New Zealand Journal of Geology and Geophysics 46, 553–563.

De Scally, F.A., Owens, I.F., 2004. Morphometric controls and geomorphic responses on fans in the Southern Alps. Earth Surface Processes and Landforms 29, 311–322.

Dikau, R., Brabb, E., Mark, R., Pike, R., 1995. Morphometric landform analysis of New Mexico. Zeitschrift für Geomorphologie Supplement Band N.F 101, 109–126.

Duvall, A., Kirby, E., Burbank, D., 2004. Tectonic and lithologic controls on bedrock channel profiles and processes in coastal California. Journal of Geophysical Research 109, F03002. doi: 10.1029/2003JF000086.

Finlayson, D.P., Montgomery, D.R., 2003. Modeling large-scale fluvial erosion in geographic information systems. Geomorphology 53, 147–164.

Finlayson, D.P., Montgomery, D.R., Hallet, B., 2002. Spatial coincidence of rapid inferred erosion with young metamorphic massifs in the Himalaya. Geology 30, 219–222.

Gabet, E.J., Pratt-Sitaula, B., Burbank, D.W., 2004. Climatic controls on hillslope angle and relief in the Himalayas. Geology 32, 629–632.

Henderson, R.D., Thompson, S.M., 1999. Extreme rainfalls in the Southern Alps of New Zealand. Journal of Hydrology New Zealand 38, 309–330.

Hovius, N., 2000. Macroscale process systems of mountain belt erosion. In: Summerfield, M.A. (Ed.), Geomorphology and Global Tectonics. Wiley, Chichester, pp. 77–105.

Hovius, N., Stark, C.P., Allen, P.A., 1997. Sediment flux from a mountain belt derived from landslide mapping. Geology 25, 231–234.

Howard, A.D., Kerby, G., 1983. Channel changes in badlands. Geological Society of America Bulletin 94, 739–752.

Hurtrez, J.E., Sol, C., Lucazeau, F., 1999. Effect of drainage area on hypsometry from an analysis of small-scale drainage basins in the Siwalik Hills Central Nepal. Earth Surface Processes and Landforms 24, 799–808.

Jamieson, S.S.R., Sinclair, H.D., Kitstein, L.A., Purves, R.S., 2004. Tectonic forcing of longitudinal valleys in the Himalaya: morphological analysis of the Ladakh Batholith. Geomorphology 58, 49–65.

Kirby, E., Whipple, K.X., Tang, W., Chen, Z., 2003. Distribution of active rock uplift along the eastern margin of the Tibetan Plateau: inferences from bedrock channel longitudinal profiles. Journal of Geophysical Research 108 (B4), 2217. doi: 10.1029/2001JB000861.

Kirkbride, M., Matthews, D., 1997. The role of fluvial and glacial erosion in landscape evolution: the Ben Ohau Range, New Zealand. Earth Surface Processes and Landforms 22, 317–327.

Kobor, J.S., Roering, J.J., 2004. Systematic variation of bedrock channel gradients in the central Oregon Coast range: implications for rock uplift and shallow landsliding. Geomorphology 62, 239–256.

Koons, P.O., 1989. The topographic evolution of mountain belts: a numerical look at the Southern Alps, New Zealand. American Journal of Science 289, 1041–1069.

Koons, P.O., 1990. The two-sided wedge in orogeny. Erosion and collision from the sand box to the Southern Alps, 528 New Zealand. Geology 18, 679–682.

Korup, O., 2005a. Distribution of landslides in southwest New Zealand. Landslides. doi:10.1007/s10346-004-0042-0.

Korup, O., 2005b. Large landslides and their effects on sediment flux in South Westland, New Zealand. Earth Surface Processes and Landforms 30, 305–323.

Korup, O., McSaveney, M.J., Davies, T.R.H., 2004. Sediment generation and delivery from large historic landslides in the Southern Alps, New Zealand. Geomorphology 61, 189–207.

Kühni, A., Pfiffner, O.A., 2001. The relief of the Swiss Alps and adjacent areas and its relation to lithology and structure: topographic analysis from a 250-m DEM. Geomorphology 41, 285–307.

Lague, D., Davy, P., 2003. Constraints on the long-term colluvial erosion law by analyzing slope–area relationships at various tectonic uplift rates in the Siwaliks Hills Nepal. Journal of Geophysical Research 108 (B2), 2129. doi: 10.1029/2002JB001893.

McKerchar, A.I., Pearson, C.P., 1989. Flood frequency in New Zealand. Publication Hydrology Centre 20. Christchurch, 88 pp.

McSaveney, M.J., 2002. Recent rockfalls and rock avalanches in Mount Cook National Park New Zealand. In: Evans, S.G., DeGraff, J.V. (Eds.), Catastrophic Landslides: Effects, Occurrence, and Mechanisms. Geological Society of America Reviews in Engineering Geology XV, pp. 35–70.

Meigs, A., Sauber, J., 2000. Southern Alaska as an example of the long-term consequences of mountain building under the influence of glaciers. Quaternary Science Reviews 19, 1543–1562.

Montgomery, D.R., 2001. Slope distributions, thresholds hillslopes, and steady-state topography. American Journal of Science 301, 432–452.

Montgomery, D.R., 2002. Valley formation by fluvial and glacial erosion. Geology 30, 1047–1050.

Montgomery, D.R., Brandon, M.T., 2002. Topographic controls on erosion rates in tectonically active mountain ranges. Earth and Planetary Science Letters 201, 481–489.

Montgomery, D.R., Greenberg, H.M., 2000. Local relief and the height of Mount Olympus. Earth Surface Processes and Landforms 25, 385–396.

Norris, R.J., Cooper, A.F., 2000. Late Quaternary slip rates and slip partitioning on the Alpine Fault, New Zealand. Journal of Structural Geology 23, 507–520.

Pike, R., 1995. Geomorphometry—progress, practice and prospect. Zeitschrift fiir Geomorphologie N.F 101, 221–238.

Rasemann, S., Schmidt, J., Schrott, L., Dikau, R., 2002. Geomorphometry in mountain terrain. In: Bishop, M., Shroder Jr., J. (Eds.), Geographic Information Science (GIScience) and Mountain Geomorphology. Praxis Scientific Publishing, Springer, Berlin.

Riquelme, R., Martinod, J., Herail, G., Darrozes, J., Charrier, R., 2003. A geomorphological approach to determining the Neogene to Recent tectonic deformation in the Coastal Cordillera of northern Chile (Atacama). Tectonophysics 361, 255–275.

Seeber, L., Gomitz, V., 1983. River profiles along the Himalayan arc as indicators of active tectonics. Tectonophysics 92, 335–367.

Schmidt, J., Dikau, R., 1999. Extracting geomorphometric attributes and objects from digital elevation models—semantics, methods, future needs. In: Dikau, R., Saurer, H. (Eds.), GIS for Earth Surface Systems—Analysis and Modelling of the Natural Environment. Schweizbart'sche Verlagsbuchhandhmg, Stuttgart, pp. 153–173.

Schmidt, K.M., Montgomery, D.R., 1995. Limits to relief. Science 270, 617–620.

Simpson, G.D.H., Cooper, A.F., Norris, R.J., 1994. Late Quatemary evolution of the Alpine Fault zone at Paringa, South Westland, New Zealand. New Zealand Joumal of Geology and Geophysics 37, 49–58.

Sklar, L., Dietrich, W.E., 1998. River longitudinal profiles and bedrock incision models: stream power and the influence of sediment supply. In: Tinkler, K.J., Wohl, E.E. (Eds.), Rivers Over Rocks: Fluvial Processes in Bedrock Channels, Geophysical Monograph Series, vol. 107. AGU, Washington, D.C, pp. 237–260.

Snyder, N.P., Whipple, K.X., Tucker, G.E., Merritts, D.J., 2003. Channel response to tectonic forcing: field analysis of stream morphology and hydrology in the Mendocino triple junction region, northern California. Geomorphology 53, 97–127.

Strahler, A.N., 1952. Hypsometric (area–altitude) analysis of erosional topography. Geological Society of America Bulletin 63, 1117–1142.

Sutherland, R., 1995. The Australia–Pacific boundary and Cenozoic plate motions in the southwest pacific: some constraints from Geosat data. Tectonics 14, 819–831.

Tippett, J.M., Kamp, P.J.J., 1995. Quantitative relationships between uplift and relief parameters for the Southern Alps, New Zealand, as determined by fission track analysis. Earth Surface Processes and Landforms 20, 153–175.

Tucker, G.E., 2004. Drainage basin sensitivity to tectonic and climatic forcing: implications of a stochastic model for the role of entrainment and erosion thresholds. Earth Surface Processes and Landforms 29, 185–205.

Wallace, W.H., 1995. New Zealand landforms. New Zealand Geographer 11, 17–27.

Wells, A., Yetton, M.D., Duncan, R.F., Stewart, G.H., 1999. Prehistoric dates of the most recent Alpine Fault earthquakes, New Zealand. Geology 27, 995–998.

Whipple, K.X., Tucker, G.E., 1999. Dynamics of the stream-power river incision model: implications for height limits of mountain ranges, landscape response timescales, and research needs. Journal of Geophysical Research 104, 17661–17674.

Whipple, K.X., 2004. Bedrock rivers and the geomorphology of active orogens. Annual Reviews in Earth and Planetary Sciences 32, 151–185.

Whitehouse, I.E., 1988. Geomorphology of the central Southern Alps, New Zealand: the interaction of plate collision and atmospheric circulation. Zeitschrift für Geomorphologie Supplement Band N.F 69, 105–116.

Yetton, M.D., Wells, A., Traylen, N.J., 1998. The probability and consequences of the next Alpine Fault earthquake. EQC Research Project 95/193. Geotech Consulting Ltd., Christchurch. 161 pp.